LETTER

doi:10.1038/nature10498

Resonances arising from hydrodynamic memory in Brownian motion

Thomas Franosch[1]*, Matthias Grimm[2,3]*, Maxim Belushkin[4], Flavio M. Mor[3], Giuseppe Foffi[4], László Forró[3] & Sylvia Jeney[2,3]

Observation of the Brownian motion of a small probe interacting with its environment provides one of the main strategies for characterizing soft matter[1–4]. Essentially, two counteracting forces govern the motion of the Brownian particle. First, the particle is driven by rapid collisions with the surrounding solvent molecules, referred to as thermal noise. Second, the friction between the particle and the viscous solvent damps its motion. Conventionally, the thermal force is assumed to be random and characterized by a Gaussian white noise spectrum. The friction is assumed to be given by the Stokes drag, suggesting that motion is overdamped at long times in particle tracking experiments, when inertia becomes negligible. However, as the particle receives momentum from the fluctuating fluid molecules, it also displaces the fluid in its immediate vicinity. The entrained fluid acts back on the particle and gives rise to long-range correlations[5,6]. This hydrodynamic 'memory' translates to thermal forces, which have a coloured, that is, non-white, noise spectrum. One hundred years after Perrin's pioneering experiments on Brownian motion[7–9], direct experimental observation of this colour is still elusive[10]. Here we measure the spectrum of thermal noise by confining the Brownian fluctuations of a microsphere in a strong optical trap. We show that hydrodynamic correlations result in a resonant peak in the power spectral density of the sphere's positional fluctuations, in strong contrast to overdamped systems. Furthermore, we demonstrate different strategies to achieve peak amplification. By analogy with microcantilever-based sensors[11,12], our results reveal that the particle–fluid–trap system can be considered a nanomechanical resonator in which the intrinsic hydrodynamic backflow enhances resonance. Therefore, instead of being treated as a disturbance, details in thermal noise could be exploited for the development of new types of sensor and particle-based assay in lab-on-a-chip applications[13,14].

Einstein's theory of Brownian motion[15], published in 1905, received considerable attention and was later reformulated in terms of a Langevin equation[16]. In it, particle motion is driven by thermal fluctuations induced through collisions with the fluid molecules. These rapid 'kicks' are assumed to be random and independent at frequencies much smaller than the collision rate of ~1 THz. The thermal force consequently has a white noise spectrum[16]; that is, the spectrum is constant over a wide range of frequencies. Momentum is transferred from the particle to the fluid at times $\tau_p = m_p/\gamma$ (Fig. 1a, left), where $\gamma = 6\pi\eta R$ is the coefficient of static friction of the particle for macroscopic no-slip boundary conditions, m_p is the particle's mass, η is the shear viscosity of the fluid and R is the radius of the particle (which is taken to be spherical). However, when the densities of the particle and the fluid, ρ_p and, respectively, ρ_f, are comparable, their coupling becomes important[17,18]. As the suspended particle fluctuates through the solvent, long-range correlations build up as a result of momentum exchange, leading to hydrodynamic memory in the solvent. Hence, an additional timescale, $\tau_f = R^2\rho_f/\eta$, which describes the time needed by the perturbed fluid flow field to diffuse over one particle radius (Fig. 1a, middle), becomes important. According to the fluctuation–dissipation theorem, the statistics of the thermal force, $F_{th}(t)$, is characterized by a delta-correlated white noise term and a coloured, frequency-dependent component that reflects the retarded viscous response of the fluid continuum to the particle.

To measure directly the predicted correlations in thermal noise, we combined strong optical trapping with high-resolution, 3D position detection[19] (Supplementary Information, section 1). The resulting force balance for the particle reads $m_p\ddot{x}(t) = F_{fr}(t) - Kx(t) + F_{th}(t)$, where $x(t)$ is the particle's displacement from the trap centre (with a dot denoting differentiation with respect to time), $F_{fr}(t)$ is the non-instantaneous friction force on the particle and K is the stiffness of the optical trap. This harmonic restoring force gives the trap relaxation time of $\tau_K = \gamma/K$ (Fig. 1a, right). At long times, strong trapping eventually dominates over friction and becomes the main force counteracting thermal excitation. The Langevin equation reduces then to $Kx(t) \approx F_{th}(t)$. Consequently, when tracking the fluctuating motion of the particle in a strong harmonic potential (Fig. 1b, c), we effectively probe the thermal force of the fluid[10]. Correlations in thermal noise

$$\langle F_{th}(t)F_{th}(0)\rangle \approx K^2\langle x(t)x(0)\rangle \qquad (1)$$

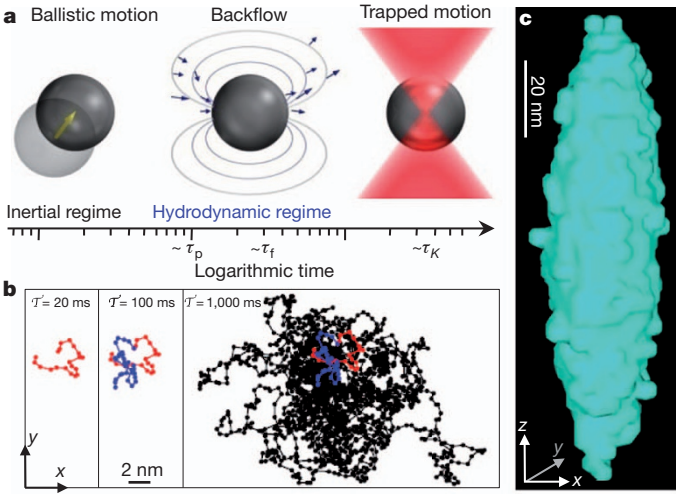

Figure 1 | Characteristic time scales of a Brownian particle confined by the three-dimensional (3D) harmonic potential of an optical trap. **a**, On very short timescales ($t \ll \tau_p$), the particle undergoes ballistic motion governed by m_p (left). On timescale τ_f, hydrodynamic backflow develops (centre; solid lines show the emerging fluid velocity field; arrows are obtained from our computer simulations). Finally, for $t \gtrsim \tau_K$, the harmonic potential of the trap sets in and confines particle diffusion (right). **b**, Trajectories of the trapped sphere measured at three different time intervals, in the dimensions, x and y, lateral to the optical axis, z. **c**, 3D position histogram of the same sphere after the measurement time $\mathcal{T} \approx 4$ ms. The small displacements of the bead are indicative of the strong trapping forces.

[1]Institut für Theoretische Physik, Friedrich-Alexander-Universität Erlangen-Nürnberg, Staudtstraße 7, 91058 Erlangen, Germany. [2]M. E. Müller Institute for Structural Biology, Biozentrum, University of Basel, Klingelbergstrasse 70, Basel 4056, Switzerland. [3]Laboratory of Physics of Complex Matter, Ecole Polytechnique Fédérale de Lausanne (EPFL), CH-1015 Lausanne, Switzerland. [4]Institute of Theoretical Physics, Ecole Polytechnique Fédérale de Lausanne (EPFL), CH-1015 Lausanne, Switzerland.
*These authors contributed equally to this work.

become directly accessible through the positional autocorrelation function, $\mathrm{PAF}(t) = \langle x(t)x(0)\rangle$, calculated from the recorded fluctuations of the trapped sphere (Fig. 1b).

The sequential order and magnitudes of the various timescales depend on the size and mass of the Brownian particle, the nature of the solvent and the stiffness of the optical trap. The experimental challenge consists of exploring a wide range of timescales. Therefore, we optimized our set-up[20] to achieve a resolution of ~1 nm in space and close to 1 μs in time (Supplementary Information, section 1). In typical optical tweezers experiments, silica or polystyrene spheres immersed in water and with sizes $\lesssim 1$ μm are used. This yields values for τ_f and τ_p of less than 1 μs, which is below our temporal resolution limit[21]. Therefore, we instead used melamine resin beads with diameters of between 2 and 3 μm and suspended them in acetone, which is three times less viscous than water. In this set-up, $\tau_p \approx 1$–3 μs and $\tau_f \approx 2$–6 μs. Furthermore, the difference between the refractive indices of resin ($n = 1.68$) and acetone ($n = 1.36$) was high enough to provide good trapping efficiency. With such an experimental configuration, we could increase τ_f and K sufficiently to bring the trap relaxation time, τ_K, close to τ_f. This made the window in which mainly thermal force correlations determine the bead's dynamics (Fig. 1a, middle) experimentally accessible. On these timescales, the mass of the particle is already negligible, leading to a clear separation between the inertial and hydrodynamic regimes of Brownian motion (Supplementary Information, section 5).

Figure 2a, b shows the mean squared displacements and positional autocorrelation functions calculated from the measured position fluctuations, $x(t)$ (Supplementary Information, section 3), of a single resin sphere immersed in water (green circles) or in acetone (blue circles) and held with comparable optical forces. $\mathrm{PAF}(t)$ has a clear zero-crossing followed by anticorrelations. The appearance of anticorrelations is in remarkable contrast with the exponential relaxation, $(k_BT/K)e^{-t/\tau_K}$, characteristic of overdamped harmonic oscillators subject to instantaneous Stokes friction $-\gamma\dot{x}(t)$. In the frequency domain (Fig. 2c), the corresponding power spectral density, $\mathrm{PSD}(f)$, shows that increasing τ_f, and hence decreasing the ratio τ_K/τ_f by reducing the fluid's viscosity, caused the emergence of a resonance. This resonant peak indicates that the thermal force spectrum is enhanced as frequency increases (blue circles). In water (green circles), the maximal corner frequency, $f_K = 1/2\pi\tau_K$, we obtained resulted in an enhancement of the PSD close to our noise limit. Nevertheless, deviations from the simple Lorentzian, $\mathrm{PSD}(f) = 2(k_BT/K)\tau_K/[1 + (2\pi f\tau_K)^2]$, of overdamped systems (green line) are clearly visible for frequencies around f_K.

For a quantitative description, we solve a Langevin equation with no-slip boundary conditions accounting for slow vortex diffusion[17,18] and trapping[22,23]. Our data (Fig. 2, symbols) are in excellent agreement with the theoretical expression (Fig. 2, black lines) over three decades in time and four orders of magnitude in signal (Fig. 2b), and we observe a hydrodynamic power-law tail, $\mathrm{PAF}(t) \approx -(k_BT\gamma/K^2)\sqrt{\tau_f/4\pi t^3}$, which by equation (1) directly reflects the corresponding persistent correlations in the thermal forces

$$\langle F_{th}(t)F_{th}(0)\rangle = -k_BT\gamma\sqrt{\tau_f/4\pi}\,t^{-3/2}$$

for times for which compressibility effects from the fluid can be ignored (Supplementary Information, section 4). The negative overshoot in the PAF and the equivalent resonant peak in the PSD originate solely from the hydrodynamic coupling between the fluid and the particle.

In the Fourier domain, positional fluctuations $\hat{x}(f) = \int x(t)e^{2\pi ift}\,dt$ are connected to the thermal forces by a linear relation, $\hat{x}(f) = \hat{G}(f)\hat{F}_{th}(f)$, where $\hat{G}(f)$ is the Fourier transform of the Green function (Supplementary Information, section 4). Consequently, $\hat{x}(f)$ is a filtered signal of the noise $\hat{F}_{th}(f)$, and the PSD of the Brownian thermal noise, $\mathrm{PSD}_{th}(f)$, is related to the measured PSD by

$$\mathrm{PSD}_{th}(f) = \left|\hat{G}(f)\right|^{-2}\mathrm{PSD}(f) \qquad (2)$$

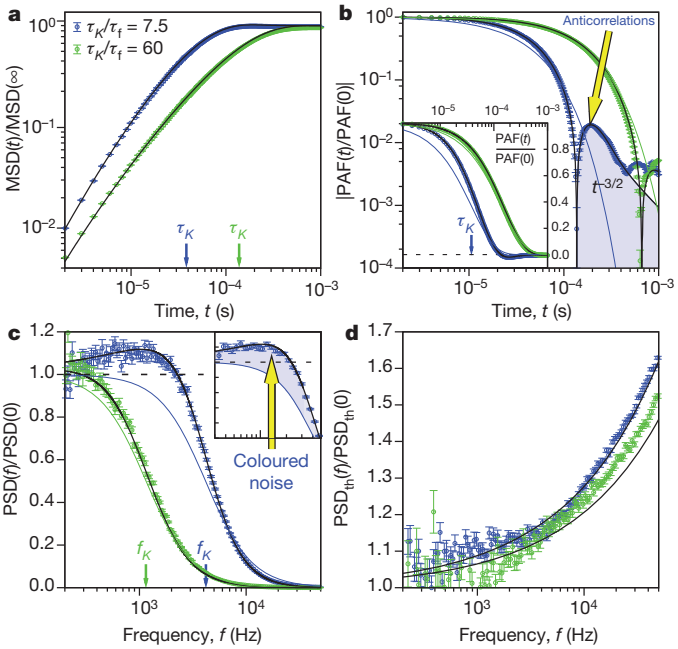

Figure 2 | The colour of thermal force. **a**, Double-logarithmic plot of the mean squared displacement (MSD) normalized to its long-time limit, $2k_BT/K$ (k_B, Boltzmann's constant), for an optically trapped ($K \approx 205$ μN m^{-1}), melamine resin sphere ($R = 1.45$ μm) in water (green circles: $\tau_f = 2.3$ μs, $\tau_K = 138.0$ μs) or acetone (blue circles: $\tau_f = 5.1$ μs, $\tau_K = 38.3$ μs). **b**, Double-logarithmic plot of the corresponding PAF(t) blocked in 100 bins per decade and normalized to its initial value, $\mathrm{PAF}(0) = k_BT/K$. The persistent anticorrelations are visible after the zero-crossing (narrow spike) and follow a $t^{-3/2}$ power-law decay. The green and blue lines indicate exponential relaxations and serve as guide to the eye. Inset, log–linear plot of the same data. **c**, Log–linear representation of the corresponding PSD blocked in 50 bins per decade and normalized to its zero-frequency value, $2k_BT\tau_K/K$. The green and blue lines are Lorentzian spectra for reference. Inset, magnified view of the enhancement of the PSD, blocked in 20 bins per decade, reflecting the colour of thermal noise. **d**, Direct representation of the PSD of F_{th} (equation (2)). The black lines correspond to the full hydrodynamic theory including inertial effects[22,23]. The parameters τ_f and τ_K were extracted from the fit to the theory. Error bars, 1 s.e. of the mean from blocking.

The data shown in Fig. 2d confirm the departure from white noise through a drastic increase in thermal noise at higher frequencies. Deviations from Gaussian white noise are towards the blue end of the spectrum at frequencies that are much smaller than the collision rate of the solvent molecules, and reflect the colour of thermal force[10].

The observed resonance in the PSD can be enhanced by decreasing the ratio τ_K/τ_f and hence increasing K. Figure 3a shows peak amplification with increasing laser power up to a stiffness of 412 μN m^{-1}. In the hydrodynamic regime, Brownian motion is strongly sensitive to particle size because the determinant timescale, τ_f, is proportional to R^2. A difference in the bead radius, ΔR, of only a few per cent results in a detectable shift in the PAF around its zero-crossing, in acetone as well as in water (Fig. 3b).

Experimental access to short timescales reveals a resonance in Brownian motion where overdamped motion is commonly assumed. For a given solvent and particle, it is possible to investigate the dynamics of the system in different regimes by decreasing τ_K and detecting the position fluctuations at the highest bandwidth. Stronger and narrower resonances can be obtained in the inertial regime, where Brownian motion is also sensitive to the particle's mass[24,25]. To reach this window, τ_K has to be brought close to τ_p by increasing K or m_p. Although heavier particles, which simultaneously allow for more efficient trapping, are still to be developed[26], the timeline displayed in Fig. 1a can be explored theoretically and by means of computer simulations. Transition to the inertial regime is marked by the appearance of a peak in the case of the

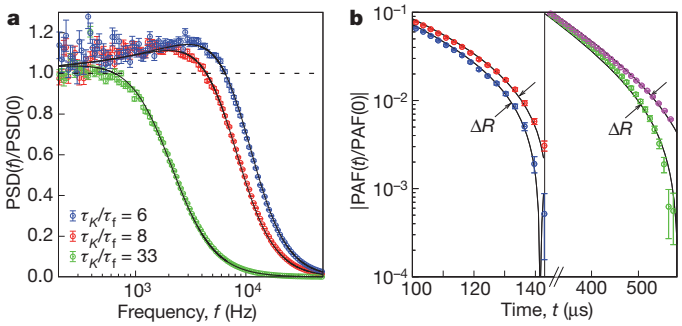

Figure 3 | Enhancing resonance and sensitivity to particle size. **a**, Log–linear representation of the normalized PSD, blocked in 50 bins per decade, of a resin sphere ($R = 1$ μm) in acetone for increasing trap stiffness (green, $K = 77$ μN m^{-1}; red, 309 μN m^{-1}; blue, 412 μN m^{-1}). **b**, Magnified view of a log–linear plot of the normalized PAF(t), blocked in 100 bins per decade, close to the zero-crossing for resin spheres of slightly different radii held by traps of the same stiffness, in acetone (blue, $R = 1.45$ μm; red, 1.35 μm; $K \approx 205$ μN m^{-1}) and water (green, 1.50 μm; magenta, 1.45 μm; $K \approx 195$ μN m^{-1}). The black lines in each plot correspond to the full hydrodynamic theory[22,23]. Data were acquired and processed as described in Fig. 2. Error bars, 1 s.e. of the mean from blocking.

harmonic oscillator with $\tau_K < 2\tau_p$. When τ_K is further decreased, the mass term in the Langevin equation eventually becomes larger than the friction term. Interestingly, in comparison with the simple harmonic oscillator (Fig. 4a, dashed lines), the peak is significantly enhanced and its position, f_{max}, is shifted to lower frequencies by the contribution of hydrodynamic memory (Fig. 4a, solid lines).

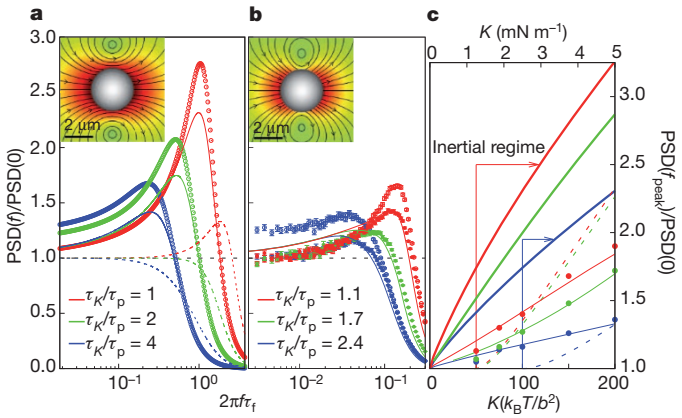

Figure 4 | Transition to the inertial regime. **a**, Theoretical PSD of a resin sphere with no-slip boundary conditions in acetone ($R = 1.5$ μm, $\tau_p = 2.3$ μs, $\tau_f = 5.4$ μs), for very strong traps (blue, $K = 1.02$ mN m^{-1}; green, 2.04 mN m^{-1}; red, 4.07 mN m^{-1}). The dashed lines show the results for a damped harmonic oscillator[16], for comparison. The coloured circles represent the corresponding PSD$_{exc}(f)$ with $g = 50\%$ and $f_{exc} \approx 2f_{peak}$. Inset, corresponding fluid velocity field developing around the sphere when moving in the x direction at $f = 1/2\pi\tau_f$. The arrows indicate the direction of the velocity field. **b**, Simulation data (filled circles) for an equivalent system with $\tau_p = 0.7\tau_f$ evaluated in a compressible fluid under full-slip conditions, $\gamma = 4\pi\eta R$. The coloured theoretical lines account for vortex diffusion, as well as for sound waves. The open circles are simulation data for an excitation with $g = 50\%$ and $f_{exc} = 2f_{max}$. Inset, corresponding fluid velocity field at $f = 1/2\pi\tau_f$, decreasing from red to green. All curves in **a** and **b** are normalized to the zero-frequency value of the respective non-excited PSD. **c**, Normalized peak height for increasing trap strength, calculated for particles of different sizes and densities in acetone, where b is the unit length of simulations (Supplementary Information, Section 7) (thick lines; blue: $2b = R = 1.0$ μm, $\rho_p = 1{,}510$ kg m^{-3}; green: $R = 1.0$ μm, $\rho_p = 3{,}020$ kg m^{-3}; red: $R = 2.0$ μm, $\rho_p = 1{,}510$ kg m^{-3}) and compared with the harmonic oscillator (dashed lines). Simulation data (symbols) are compared to the corresponding theory (thin lines).

The study of Brownian motion on short timescales in a medium with hydrodynamic effects has also become accessible by advanced simulation techniques. We used multiparticle collision dynamics (see ref. 27 and references therein) with molecular dynamics coupling between solute and solvent particles. The method yielded a compressible solvent and correctly reflected the hydrodynamic effects at coarse-grained scales. The approach was implemented most conveniently for full-slip boundary conditions at the solute–solvent interface, whereas our experiments obeyed no-slip conditions. The simulation results for the PSD show that a resonance emerges in the hydrodynamic regime as well as in the inertial regime (Fig. 4b, filled circles), irrespective of boundary conditions at the solvent–solute interface. However, the weak coupling between the Brownian particle and the surrounding fluid yielded a resonance much weaker than that which emerged under no-slip conditions (Fig. 4a). The collected data follow the theoretical curves (Fig. 4b, coloured lines), where friction is evaluated for a compressible fluid under full-slip conditions (Supplementary Information, sections 4 and 7).

The enhanced resonance is sensitive to the size of the bead in the hydrodynamic regime (Fig. 4c, red curves versus green and blue curves). Also, it is mass sensitive in the inertial regime of the simulation and, more markedly, under experimental conditions. In contrast, for the harmonic oscillator, sensitivity to particle size is much lower and sensitivity to its mass occurs only in the underdamped regime, where $\tau_K < 2\tau_p$ (Fig. 4c, dashed lines).

Additional peak amplification can be achieved through parametric resonance[25,28,29] by periodically modulating the trap strength at frequency f_{exc}: $K(t) = K[1 + g\cos(2\pi f_{exc}t)]$. We obtained the theoretical excited PSD, PSD$_{exc}(f)$, normalized to the initial value of the non-excited PSD, from the solution of a parametrically modulated Langevin equation, including hydrodynamic memory, using second-order perturbation theory in the reduced modulation amplitude, g (Supplementary Information, section 6). As for a harmonic oscillator, also in the presence of coloured friction, the greatest additional peak amplification is achieved at a frequency of $f_{exc} \approx 2f_{peak}$, which yields an increase of up to 20% when $g = 50\%$ (Fig. 4a, open circles). Comparable results were obtained with computer simulations (Fig. 4b, open circles).

Exploiting the hydrodynamic and inertial regimes of Brownian motion for particle-based assays will become a common technological approach[13,14]. We anticipate that changes in the particle's morphology, such as swelling or a reaction occurring at its surface, will alter short-time dynamics and become detectable. As single cells, microorganisms and microcarriers can also be bound harmonically[12,30], short-time detection of their Brownian fluctuations may become a sensitive way to characterize their state or evolution in native solutions and without specific markers. Reciprocally, changes in the medium surrounding the probing particle modulate the particle's fluctuation spectrum[2–4], offering a means of studying dynamic polymer systems in great detail.

METHODS SUMMARY

Melamine resin microspheres ($\rho_p = 1{,}510$ kg m^{-3}, $R = 1.5$, 1.45, 1.35 or 1 μm) were suspended in high-purity acetone ($\eta = 0.32$ cP (1 cP = 1 mPa s), $\rho_f = 790$ kg m^{-3}) or water ($\eta = 0.95$ cP, $\rho_f = 1{,}000$ kg m^{-3}) at minimal concentrations to allow trapping and observation of a single particle. After loading, the sample chamber was mounted onto the 3D piezo stage of our custom-made inverted microscope/optical trap set-up[20]. A bead was trapped in the focus of a Gaussian trapping beam produced by a diode-pumped, ultralow-noise Nd:YAG laser with a wavelength of $\lambda = 1{,}064$ nm and a maximal output power of 500 mW in continuous-wave mode. At the focus, the remaining power was measured to be 200 mW for the stiffest traps used. To avoid surface effects, the trapped bead was brought by the piezo stage no closer than 40 μm to the top or bottom glass surface of our sample chambers, which were more than 100 μm thick. Fluctuations in the position of the bead were detected in 3D by an InGaAs quadrant photodiode[31] with a diameter of 2.0 mm. The signals from the quadrant photodiode were fed into a custom-built preamplifier, which provided two differential signals between the photodiode quadrants, giving the fluctuations in the x and y directions, and one signal that is proportional to the

total light intensity, yielding the fluctuation in the direction parallel to the optical axis, z. Subsequently, we used differential amplifiers to adjust the preamplifier signals for optimal digitalization by the data acquisition board with a dynamic range of 12 bits. All data were collected for $\mathcal{T} \approx 50$ s at a sampling rate of 1 MHz, corresponding to $\sim 5 \times 10^7$ data points. The PSD presented in Figs 2 and 3 were computed from overlapping windows of 2^{22} points.

Received 31 January; accepted 18 August 2011.

1. Mason, T. G. & Weitz, D. A. Optical measurements of frequency-dependent linear viscoelastic moduli of complex fluids. *Phys. Rev. Lett.* **74,** 1250–1253 (1995).
2. Nowak, A. P. *et al.* Rapidly recovering hydrogel scaffolds from self-assembling diblock copolypeptide amphiphiles. *Nature* **417,** 424–428 (2002).
3. Gardel, M. L. *et al.* Elastic behavior of cross-linked and bundled actin networks. *Science* **304,** 1301–1305 (2004).
4. Chaudhuri, O., Parekh, S. H. & Fletcher, D. A. Reversible stress softening of actin networks. *Nature* **445,** 295–298 (2007).
5. Alder, B. J. & Wainwright, T. E. Velocity autocorrelations for hard spheres. *Phys. Rev. Lett.* **18,** 988–990 (1967).
6. Jeney, S., Lukić, B., Kraus, J. A., Franosch, T. & Forró, L. Anisotropic memory effects in confined colloidal diffusion. *Phys. Rev. Lett.* **100,** 240604 (2008).
7. Perrin, J. Mouvement brownien et réalité moléculaire. *Ann. Chim. Phys.* **18,** 1–114 (1909).
8. Perrin, J. *Atoms* Ch. 3–5 (Constable, 1920).
9. Hänggi, P. & Marchesoni, F. 100 years of Brownian motion. *Chaos* **15,** 026101 (2005).
10. Berg-Sørensen, K. & Flyvbjerg, H. The colour of thermal noise in classical Brownian motion: a feasibility study of direct experimental observation. *N. J. Phys.* **7,** 38 (2005).
11. Fritz, J. *et al.* Translating biomolecular recognition into nanomechanics. *Science* **288,** 316–318 (2000).
12. Burg, T. P. *et al.* Weighing of biomolecules, single cells and single nanoparticles in fluid. *Nature* **446,** 1066–1069 (2007).
13. Braeckmans, K., De Smedt, S. C., Leblans, M., Pauwels, R. & Demeester, J. Encoding microcarriers: present and future technologies. *Nature Rev. Drug Discov.* **1,** 447–456 (2002).
14. Craighead, H. Future lab-on-a-chip technologies for interrogating individual molecules. *Nature* **442,** 387–393 (2006).
15. Einstein, A. Über die von der molekularkinetischen Theorie der Wärme geforderte Bewegung von in ruhenden Flüssigkeiten suspendierten Teilchen. *Ann. Phys.* **322,** 549–560 (1905).
16. Wang, M. C. & Uhlenbeck, G. E. On the theory of the Brownian motion II. *Rev. Mod. Phys.* **17,** 323–342 (1945).
17. Vladimirsky, V. & Terletzky, Y. A. Hydrodynamical theory of translational Brownian motion. *Zh. Eksp. Theor. Fiz.* **15,** 258–263 (1945).
18. Hinch, E. J. Application of the Langevin equation to fluid suspensions. *J. Fluid Mech.* **72,** 499–511 (1975).
19. Pralle, A., Prummer, M., Florin, E.-L., Stelzer, E. H. K. & Horber, J. K. H. Three-dimensional high-resolution particle tracking for optical tweezers by forward scattered light. *Microsc. Res. Tech.* **44,** 378–386 (1999).
20. Jeney, S., Mor, F., Kőszali, R., Forró, L. & Moy, V. T. Monitoring ligand-receptor interactions by photonic force microscopy. *Nanotechnology* **21,** 255102 (2010).
21. Lukić, B. *et al.* Motion of a colloidal particle in an optical trap. *Phys. Rev. E* **76,** 011112 (2007).
22. Berg-Sørensen, K. & Flyvbjerg, H. Power spectrum analysis for optical tweezers. *Rev. Sci. Instrum.* **75,** 594–612 (2004).
23. Clercx, H. J. H. & Schram, P. P. J. M. Brownian particles in shear flow and harmonic potentials: a study of long-time tails. *Phys. Rev. A* **46,** 1942–1950 (1992).
24. Huang, R. *et al.* Direct observation of the full transition from ballistic to diffusive Brownian motion in a liquid. *Nature Phys.* **7,** 576–580 (2011).
25. Di Leonardo, R. *et al.* Parametric resonance of optically trapped aerosols. *Phys. Rev. Lett.* **99,** 010601 (2007).
26. Bormuth, V. *et al.* Optical trapping of coated microspheres. *Opt. Express* **16,** 13831–13844 (2008).
27. Gompper, G., Ihle, T., Kroll, D. M. & Winkler, R. G. Advanced computer simulation approaches for soft matter sciences III. *Adv. Polym. Sci.* **221,** 1–87 (2009).
28. Zerbe, C., Jung, P. & Hänggi, P. Brownian parametric oscillators. *Phys. Rev. E* **49,** 3626–3635 (1994).
29. Pedersen, L. & Flyvbjerg, H. Comment on ''Direct measurement of the oscillation frequency in an optical-tweezers trap by parametric excitation''. *Phys. Rev. Lett.* **98,** 189801 (2007).
30. Ashkin, A., Dziedzic, J. M. & Yamane, T. Optical trapping and manipulation of single cells using infrared laser beams. *Nature* **330,** 769–771 (1987).
31. Peterman, E. J. G., van Dijk, M. A., Kapitein, L. C. & Schmidt, C. F. Extending the bandwidth of optical-tweezers interferometry. *Rev. Sci. Instrum.* **74,** 3246–3249 (2003).

Supplementary Information is linked to the online version of the paper at www.nature.com/nature.

Acknowledgements S.J. acknowledges the Swiss National Science Foundation (SNF; grant nos 200021-113529 and 206021-121396). M.G. is supported by NCCR Nanoscale Science and the German Academic Exchange Service (DAAD) and F.M.M. is supported by the National Competence Center in Biomedical Imaging (NCCBI). M.B. and G.F. acknowledge support from the SNF (grant no. PP0022_119006). We thank W. Öffner and R. Kőszali for technical help and U. Aebi, B. U. Felderhof, H. Flyvbjerg, S. Melchionna, E. Sackmann and R. G. Winkler for discussions.

Author Contributions T.F. and M.G. contributed to the planning of the experiments, designed parts of the data analysis software, derived the theory, fitted the theory to the data and interpreted the data. M.B. performed the simulations, analysed the numerical results and contributed to the fitting of the data. F.M.M. contributed to the optimization of the experimental set-up. M.B. and G.F. devised, implemented and tested the numerical simulations. L.F. contributed to the planning of the experiments. S.J. constructed and characterized the experimental set-up; designed, planned and carried out the experiments; designed the data analysis software; and interpreted the data. All authors contributed to, discussed and commented on the manuscript.

Author Information Reprints and permissions information is available at www.nature.com/reprints. The authors declare no competing financial interests. Readers are welcome to comment on the online version of this article at www.nature.com/nature. Correspondence and requests for materials should be addressed to S.J. (sylvia.jeney@epfl.ch).